molecular pharmaceutics

Article

pubs.acs.org/molecularpharmaceutics

A New Insight for an Old System: Protein-PEG Colocalization in Relation to Protein Release from PCL/PEG Blends

Kerh Lin Liu,[†] Effendi Widjaja,[‡] Yingying Huang,[†] Xu Wen Ng,[†] Say Chye Joachim Loo,[†] Freddy Yin Chiang Boey,[†] and Subbu S. Venkatraman*,[†]

[†]School of Materials Science and Engineering, Nanyang Technological University, Block N4.1-02-06, Nanyang Avenue, Singapore 639798

[‡]Institute of Chemical and Engineering Sciences, 1 Pesek Road, Jurong Island, Singapore 627833

Supporting Information

ABSTRACT: Quantification of protein−polymer colocalization in a phase-separated polymer blend gives important insights into the protein release mechanism. Here, we report on the first visualization of protein-poly(ethylene glycol) (protein-PEG) colocalization in poly(ε-caprolactone)/poly(ethylene glycol) (PCL/PEG) blend films using a combined application of confocal Raman mapping and confocal laser scanning microscopy (CLSM) imaging. The degree of protein-PEG colocalization was further quantified via a novel image processing technique. This technique also allowed us to characterize the 3-D protein distribution within the films. Our results showed that the proteins were homogeneously distributed within the film matrix, independent of PEG content. However, the degree of protein-PEG colocalization was inversely proportional to PEG content, ranging from 65 to 94%. This quantitative data on protein-PEG colocalization was used along with in vitro PEG leaching profile to construct a predictive model for overall protein release. Our prediction matched well with the experimental protein release profile, which is characterized by an initial burst release and a subsequent slower diffusional release. More importantly, the success of this predictive model has highlighted the influence of protein-PEG colocalization on the protein release mechanism.

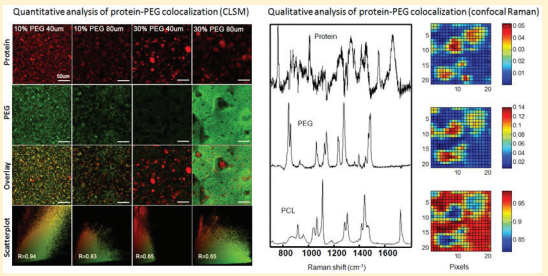

KEYWORDS: *colocalization, partitioning, image processing, distribution, protein release*

INTRODUCTION

A simple approach to modify release rates of a drug or protein from a biodegradable polymer is through blending. The advantages of polymer blends for controlled release applications include easy fabrication of devices and manipulation of device properties such as hydration rate, degradation rate and drug loading. The earlier works to investigate drug/protein release mechanisms involved the measurement of water uptake in PCL/PEG tablet[1] and PLA/PEG microspheres.[2] In these studies, the hydrophilic PEG was dissolved in the release medium, resulting in the formation of swollen structure with high water content, which subsequently increased the drug/protein release rate. On the other hand, others use scanning electron microscopy (SEM) to observe the change in matrix porosity in PLGA/PEG microspheres,[3] PLA/PEG microspheres,[2] PCL/PEG tablet,[4] and fibers.[5] In these studies, PEG acted as a pore former, where the matrix porosity increases with PEG content at the end of the release studies. It was proposed that the PEG aggregates presented on the surfaces were dissolved and leached out from the matrix when contacted with an aqueous medium; pores were consequently formed to allow drug/protein release. More recent studies involved the measurement of PEG leaching rate together with drug/protein release rate from a variety of PEG blend systems such as lipid/PEG[6−9] and ethylcellulose/PEG[10] blends. Koennings et al.[9] proposed a parallel release of PEG and protein (also pore formation related), as the PEG release profile corresponds closely to the protein release profile. Another group of researchers[6−8] fitted a mathematical model based on Fick's second law of diffusion to calculate the diffusion coefficient of protein and PEG. As a result, they discovered a nonconstant protein diffusion coefficient. Their proposed protein release mechanism is as follows: the simultaneous dissolution and diffusion of PEG increase the porosity of the matrices, therefore increasing the diffusivity of protein (the mobility of protein molecules increases with increasing porosity), which subsequently increases the overall protein release.

Despite the extensive studies of PEG blend systems, the release mechanisms remain uncertain due to the intrinsic immiscibility of most polymers that causes phase separation during solvent casting in film preparation.[11−13] Furthermore, the use of a hydrophilic polymer may lead to fast polymer leaching[4,5,7,8,10,14−16] that complicates the release mechanisms.

Received: November 17, 2010
Accepted: October 30, 2011
Published: October 31, 2011

Table 1. Composition of the Prepared Formulations and Their Corresponding Usage

sample name	polymer ratio (%)			protein loading (wt % of total film)		film thickness (μm)
	PCL	PEG	FITC-PEG	lysozyme	rhodamine B- lysozyme	
In Vitro Protein Release and Raman Mapping for Qualitative Analysis						
PCL 80 μm	100			3		80
10% PEG 80 μm	90	10		3		80
30% PEG 80 μm	70	30		3		80
PCL 40 μm	100			3		40
10% PEG 40 μm	90	10		3		40
30% PEG 40 μm	70	30		3		40
PEG Leaching and CLSM Imaging for Quantitative Analysis						
10% FITC-PEG 80 μm	90		10		3	80
30% FITC-PEG 80 μm	70		30		3	80
10% FITC-PEG 40 μm	90		10		3	40
30% FITC-PEG 40 μm	70		30		3	40

In particular, it has been almost impossible to quantify the preferential partitioning of drug/protein into each of the phases and thus to understand how this partitioning affects the drug/protein release. To achieve this quantification, we employed high lateral and depth resolution techniques.

The quantification methods currently available for drug distribution studies are limited to surface analysis. Belu and coworkers[17] utilized electron spectroscopy for chemical analysis (ESCA) to quantify the surface compositions of rapamycin on a coated stent with a detection depth limited to ~10 nm. X-ray photoelectron spectroscopy (XPS) depth profiling was used by Rafati et al. to ascertain quantitative weight concentration of drug loaded PLA films at depth of 96 nm.[18] Although valuable, the low penetration depths for these instruments limit their application for a wide variety of drug delivery systems; such as polymeric degradable films[19,20] and polymeric-coated drug-eluting stents[21] where the carrier thickness ranged from 10 μm to 160 μm.

Confocal Raman microscopy, which has a very high spatial resolution and is noninvasive, may be used to advantage this quantification. Recent Raman imaging work employed coherent anti-Stokes Raman scattering (CARS) to monitor the release of paclitaxel from polymer films,[22,23] while Windbergs et al. performed a real time theophylline anhydrate dissolution to visualize the solid-state properties of lipid-based oral dosage forms.[24] While CLSM, also nondestructive, has been extensively used and well accepted for research in cell biology,[25] its application to characterize pharmaceutical systems, in contrast, has been far less documented. Recently, Pygall et al.[26] highlighted the imaging capabilities of CLSM to study a range of pharmaceutical systems, one of which involved mapping the distribution of component within a polymer blend.[27] Other groups used CLSM to qualitatively investigate the distribution of fluorescently labeled protein in microspheres.[28,29] However, very little, if any, quantitative work has been done to fully enhance the 3-D information of CLSM images in drug delivery formulation research.

This work outlines a new paradigm that permits the prediction of protein release from a polymer blend system by the combined use of CLSM and confocal Raman imaging. We have selected a model protein (lysozyme) and a blend of commonly used polymers in the medical device industry, PCL and PEG, as the carrier film. The major objectives of this study are (1) preparation and characterization of protein loaded PCL/PEG blends, (2) quantification of protein distribution and protein-PEG colocalization via a novel image processing technique, and (3) prediction and measurement of the protein release profile. The CLSM image processing approach was used to extract important quantitative information in the microenvironment of the blend and to better understand the protein release mechanisms.

MATERIALS AND METHODS

Materials. Granular PCL (M_n 80,000 g/mol, Aldrich), PEG (M_w 2,000 g/mol, Merck-Schuchardt), lysozyme from chicken egg white (sigma), fluorescein isothiocyanate tagged PEG (FITC-PEG, M_w 2,000 g/mol, Nanocs Inc.), rhodamine B-labeled lysozyme (M_w 14.7 kDa, Nanocs Inc.), micro-bicinchoninic acid (BCA) protein assay kit (Thermo Scientific) and phosphate buffer (pH 7.4, OHME Scientific) were used as received. Dichloromethane (DCM, Tedia Chemical Company Inc.) used was of HPLC grade.

Film Preparation. PCL pellets were dissolved in DCM at 0.4 g/mL and stirred overnight to obtain homogeneous polymer solutions while lysozyme was dissolved in water at 0.2 mg/μL. For PCL/PEG blends, PEG flakes of 10 wt % and 30 wt % were codissolved with PCL in DCM at the same polymer−solvent concentration. Later, lysozyme aqueous solution was added into the PCL or PCL/PEG solutions, and was stirred for 1 h to form a single emulsion. The solutions were casted on a glass plate at the dimension of 5 cm ×20 cm and dried under ambient conditions overnight before drying in a vacuum oven at 37 °C for 1 week. Films that were used for CLSM imaging and PEG leaching experiments were prepared in the same way using rhodamine B-tagged lysozyme and FITC-tagged PEG. All the formulations are listed in Table 1.

Thermal Properties. The miscibility of PCL and PEG was investigated using differential scanning calorimetry (DSC). An indium calibrated TA Instruments DSC Q-10 was used to measure the melting temperature (T_m) of PCL and PCL/PEG blends. Samples of 5−10 mg were crimped in a standard aluminum pan with an inverted cover. The following steps were performed for thermal properties measurement: the samples were heated from −90 to 160 °C at 10 °C/min and were held isothermally for 5 min. The samples were then cooled slowly back to −90 °C at the cooling rate of 5 °C/min and were subsequently heated again to 160 at 10 °C/min. The measurements were conducted with dry nitrogen as purging gas at a flow rate of 50 mL/min.

Qualitative Analysis of Protein Distribution Using Confocal Raman Microscopy. Raman point-by-point mapping measurements were performed using a confocal Raman

microscope (InVia Reflex, Renishaw) equipped with a near-infrared enhanced, deep-depleted thermoelectrically (Peltier) cooled CCD array detector (576 × 384 pixels) and a high grade Leica microscope. The area size for each mapping was 100 μm × 100 μm with a step size of 5 μm in both the *x*- and *y*-directions. The sample was irradiated at ∼50 mW with a 785 nm near-infrared diode laser, and the backscattered light was collected with a 50× objective lens (NA 0.5). Measurement scans were collected using a static 1800 groove per mm dispersive grating in a spectral window from 700 to 1800 cm^{-1}, and the acquisition time for each spectrum was around 30 s. Spectral preprocessing that includes first spike removal due to the presence of cosmic rays and then spectral baseline correction before the collected data was further analyzed using the band-target entropy minimization (BTEM) algorithm.[30]

Raman Spectral Construction. The preprocessed Raman mapping data was analyzed using the BTEM algorithm in order to reconstruct the pure component spectra of the underlying constituents from a set of mixture spectra without recourse to any prior known spectral libraries. This algorithm has been proven well to reconstruct the pure component spectra of minor components.[31−33] When all normalized pure component spectra of all constituents have been reconstructed, the relative contributions of each constituent can be calculated by projecting them back onto the baseline-corrected and normalized data set. The spatial distribution of each constituent can thus be generated. For a more detailed description of this algorithm, readers are referred to the previous work.[30]

Quantitative Analysis of Protein Distribution Using CLSM. Protein distribution was acquired by scanning across dual channel images of FITC-PEG and rhodamine B-lysozyme loaded film in a 2-D fashion at scanned area of 246 μm × 246 μm. By repeating the same process at depth interval of 0.1 μm for the entire film thickness, a 3-D distribution profile could be constructed. A Leica TCS SP5 confocal microscope equipped with a Leica DMI 6000 CS inverted microscope was used. Ar ion laser 488 nm line and a 543 nm line were used to excite FITC and rhodamine B, respectively. The resulting emissions were collected with a HCX PL APO lambda blue 63× oil objective lens (NA 1.4). Laser power and detection gain were adjusted so that the level of autofluorescence was insignificant. Sequential scanning mode was used to remedy the problem of emission cross talk, and this was checked by acquiring dual channel images of film with single fluorophore (either FITC-PEG or rhodamine B-labeled lysozyme). No detectable cross talk was observed for these experiments. Due to the limit of penetration depth (∼25 μm within the bulk) and possible signal losses along the *z*-direction, protein and PEG distribution were characterized by scanning the film from both surfaces.

Quantification of Protein-PEG Colocalization. Colocalization of a system can be visualized using three images consisting of dual channel images, and a third overlay image generated from the combined channels where overlapping pixels turn to yellow. The presence of yellow spots is highly dependent on the relative signal intensity collected in both channels, and the overlay image will only give a reliable representation of colocalization when the signal strengths of the two imaging fluorochromes are equal.[34] As a consequence, image processing is required to evaluate the color components of the selected pair of channels. Raw images acquired by CLSM were exported to Image Pro Plus Version 4.5 in TIFF format. The dual color images first underwent background subtraction and were then subjected to RGB channel assignment before quantitative analysis. The degree of overlap was described by a few coefficients with different sensitivity and applicability: *Pearson's correlation coefficient* (R_r)[35] describes the degree of overlap between two patterns. The values of this correlation range between −1 and 1, where −1 indicates complete negative correlation, 0 indicates no significant correlation and 1 indicates perfect image registration. *Overlap coefficient according to Manders* (R)[36] indicates an overlap of the signals and thus represents the true degree of colocalization. Its value ranges from 0 to 1, the former corresponding to nonoverlapping pixels and the latter reflecting 100% colocalization between pixels of both images. *Overlap coefficients* (k_1 and k_2)[36] describe the differences in intensities of two channels. No fixed value is applicable for k_1 and k_2.

Quantification of Protein Distribution. For morphometric analysis, the images in TIFF format underwent image enhancement and were then filtered by a Flatten filter. All images were processed in the same manner before the selection of protein-rich domains, using a pseudoautomated adaptive thresholding process based on the image intensity histogram. Once all the desired domains were selected, "area" descriptor was calculated to allow the quantification of protein-rich domain at selected optical layers. The amount of protein coverage (in terms of area) at these optical layers can be estimated by the following equation:

$$\text{protein coverage per layer (\%)} = \frac{\text{total area of protein rich domain } (\mu m^2)}{\text{known image scanned area } (246\ \mu m \times 246\ \mu m)} \times 100$$

In Vitro Release Studies. In vitro release studies were conducted in two separate experiments: one was to measure the amount of protein release (A), while another was to characterize the amount of FITC-PEG leaching (B). The release studies were conducted by incubating the films of 15 × 15 mm in a rested condition at 37 °C in glass bottles, each containing 3 mL of phosphate buffer solution (57 mM KH_2PO_4, 250 mM Na_2HPO_4, pH 7.4). At each sample retrieval time point, the release medium was completely removed and replaced with fresh buffer to maintain sink condition. Protein concentration in the release medium (A) was analyzed using micro-BCA protein assay. Conversely, the amount of FITC-PEG release (B) was measured using a microplate reader (Tecan infinite M200) at the following settings: excitation wavelength = 495 nm, emission wavelength = 521 nm, and gain = 50. (For FITC-PEG standard calibration curve, readers are referred to Figure S1in the Supporting Information). All samples were prepared and tested in triplicate (n = 3) while the data is presented as mean ± standard deviation of the mean.

Statistical Analysis. A two-tailed Student *t*-test (Microsoft Excel) followed by goodness-of-fit test (Matlab) were used to compare the differences between the actual and estimated protein release profiles at all time points. The probability value $p > 0.05$ was considered to indicate statistical insignificance.

RESULTS

Polymer Miscibility. Figure 1 shows DSC traces of pure PEG crystal, protein loaded PCL film, and protein loaded PCL/PEG blends with various constituent compositions. The first

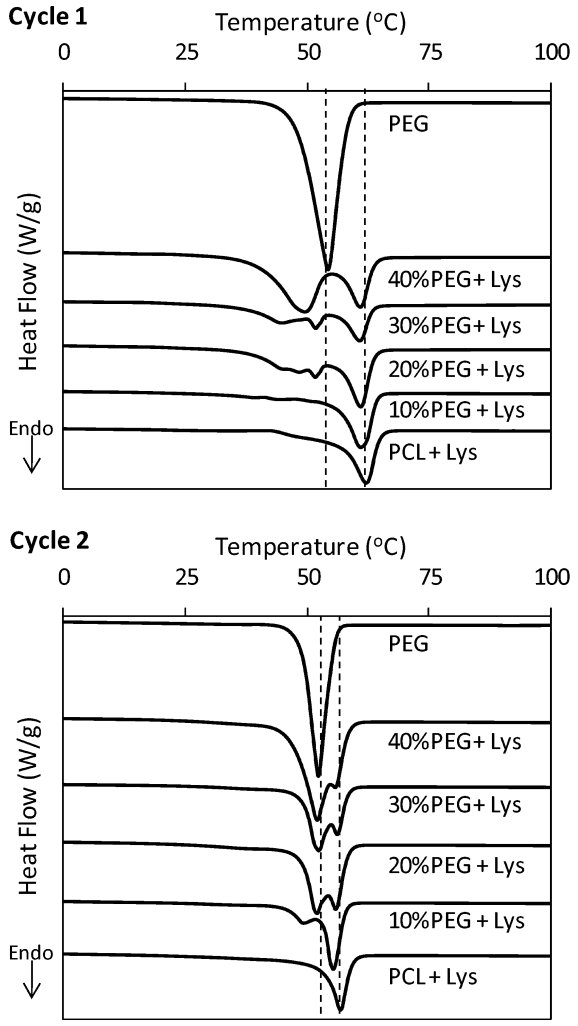

Figure 1. DSC thermograms of PCL, PEG, and their blends.

heating scan shows a sharp endothermic peak at ~54 °C and a broad endothermic peak at ~62 °C, which represent the melting temperature of pure PEG crystal and protein loaded PCL film, respectively. Their blends, however, show a more complicated behavior. Phase separation between PCL and PEG can be clearly observed with a distinguishable PCL melting peak, and a multimodal PEG melting peak at lower melting temperature. These multiple PEG endothermic peaks could be due to different crystallite types in the as-formed PEG phase in the film, as these multiple peaks disappear in the second heating scan. In the second heating scan, melting peaks of PEG and PCL are observed at 52 and 56 °C, respectively. These endothermic peaks could also be seen in their blends with different areas corresponding to the blend compositions without significant peak shifts, thus confirming that PCL and PEG crystalline phases are separate.

Qualitative Analysis of Protein-PEG Colocalization. Figure 2a shows the mapping area of the bottom surface of an 80 μm film containing 10% PEG. The development of sharp Raman peaks during the polymer crystallization is well-known for PCL and PEG. The Raman shift at 1724 cm^{-1} represents carbonyl stretching ν(C═O) of the ester group in crystalline phases of PCL,[37−40] while the sharp band splitting in the 846−862 cm^{-1} region is a characteristic band for crystalline PEG that represents symmetric CH_2 rocking and COC stretching ($r(CH_2)_s + \nu(COC)_s$) of PEG[41,42] (Figure 2b). On the other hand, the reconstructed Raman spectral estimate of lysozyme via BTEM analysis concurs well with the other literature,[43] where the strong and broad Raman bands at 1255 and 1665 cm^{-1} correspond to the amide III and amide I bands, respectively.

These three BTEM spectral estimates (protein, PEG, and PCL) were then fitted back into the original Raman mapping data set in order to determine the associated spatial distribution (Figure 2c). The color-coded scale (dimensionless) in the mapped image represents the intensities of score image of each observed component, in which the summation of the intensities of all components at each pixel is equal to unity. These score images are used to show the spatial distribution for protein, PEG, and PCL in the mapping area. The spatial distributions of these three components clearly show that there is phase segregation between PCL and PEG, and between PCL and protein. Interestingly, the spatial distributions of both the lysozyme and PEG are observed to be similar. This confirms the extensive colocalization of lysozyme and PEG in the same domain. Similar observation was found in other formulations (results not shown). However, the colocalization visualization is only qualitative using this method.

Quantitative Assessment of Protein-PEG Colocalization. Figure 3 shows dual channel images acquired by CLSM, where the red pixels represent protein distribution while the green pixels represent PEG distribution. The overlap between protein and PEG in the overlay image is shown as yellow regions, a result of the overlapped green and red pixels. This observation of colocalization was consistent with the Raman mapping images and was supported by their corresponding scatterplots. In the scatterplot, pure red and pure green pixels cluster toward the axes of the plot, while colocalized pixels that appear as orange and yellow hotspots scatter diagonally toward the upper right-hand corner. The degree of protein-PEG colocalization was quantified and listed in Table 2. Coefficients calculated for 10% PEG blends at 40 and 80 μm were $R_r = 0.83$ and 0.64, $R = 0.94$ and 0.83 (represented as 94% and 83% colocalization). On the other hand, the calculated coefficients for 30% PEG blends were $R_r = -0.15$ and −0.11, $R = 0.65$ and 0.65 for 40 and 80 μm, respectively. Overlap coefficients k_1 and k_2 show the contribution of protein and PEG to colocalization, i.e. equal contribution from both red and green channel for all the formulations except for 30% PEG (80 μm) where $k_1 \ll k_2$.

Quantitative Assessment of Protein Distribution. For each formulation, the protein coverage at a few selected optical layers was quantified. Figure 4 showed homogeneous protein distribution for all formulations, where the area coverage of protein-rich domains ranged from 8% to 35% of the total scanned area. No sign of surface segregation was observed. The protein coverage for 40 μm films was found to be slightly higher for PCL and 10% PEG films in comparison with the 80 μm formulations of the same PEG loading. However, for 30% PEG loading, the difference seems minute.

In Vitro Release. Protein released from PCL and PCL/PEG blend films was compared based on the same protein loading (Figure 5a), for two different film thicknesses. The release profiles for all the cases consist of two stages: an initial burst effect followed by a diffusional-controlled slow release. In the first stage, an initial burst of up to 35% was observed for the 30% PEG blends while lower bursts occurred for 10% PEG blends. After this initial burst, a slower diffusion-controlled release that contributed to a gradual increase of 7−10% in the

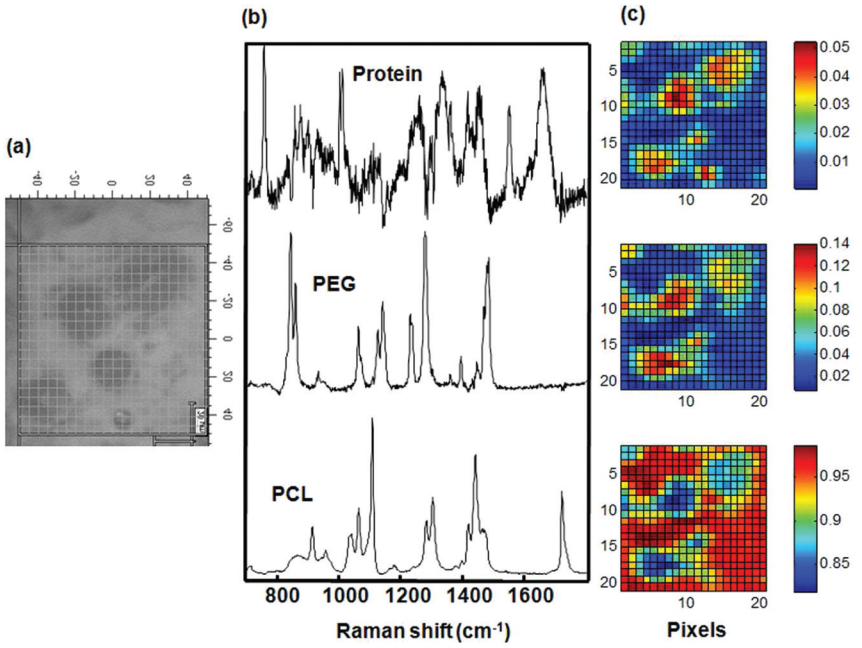

Figure 2. Raman mapping of the bottom surface of 10% PEG 80 μm film: (a) optical image of the scanned area, (b) BTEM spectral estimates for all components, and (c) their corresponding spatial distributions on the mapping area. The color-coded scale next to the mapped area represents the intensities of score image of each component.

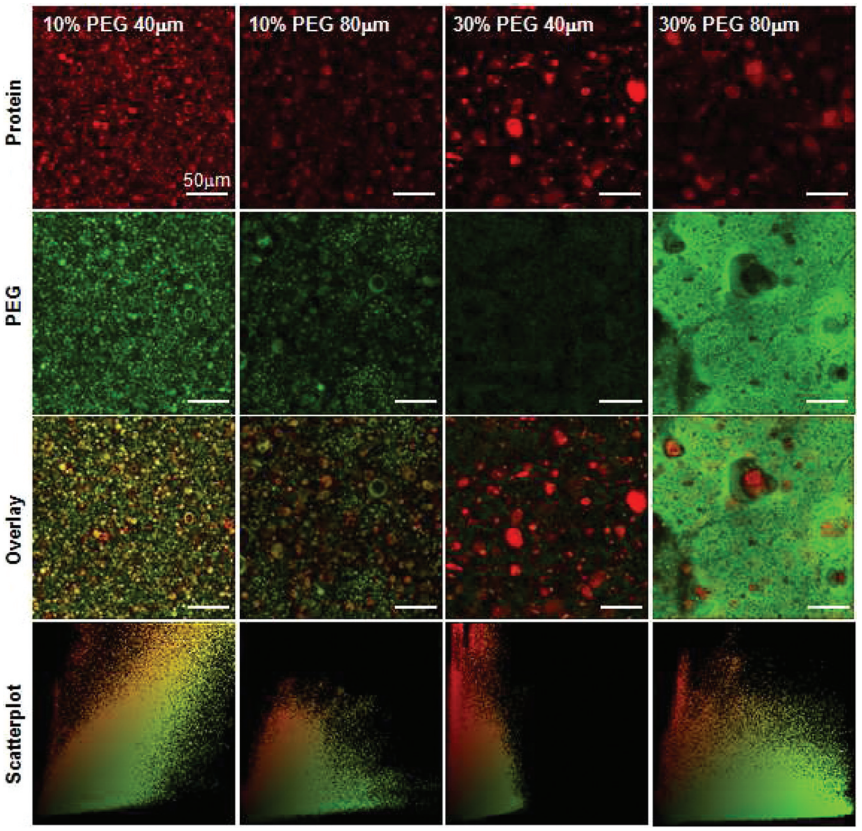

Figure 3. Dual channels (red and green) and overlay CLSM images along with their corresponding scatterplots for PCL/PEG blend films.

protein cumulative release for all formulations was observed. Protein-loaded PCL films exhibit a similar release profile, but with a much lower burst release. The effect of film thickness on the protein release rate was also compared for the 3 blend ratios. All 40 μm films exhibited a faster initial release than the 80 μm films. This is likely due to the higher water penetration rate into the thinner films, which in turn accelerates PEG leaching.

The amount of PEG leaching from PCL/PEG films is shown in Figure 5b. It is obvious that a very high amount of PEG was

dx.doi.org/10.1021/mp200513b|*Mol. Pharmaceutics* 2011, 8, 2173–2182

Table 2. Comparison of Colocalization Parameters Calculated from Dual Channel Images in Figure 3 (Mean ± Standard Deviation, n = 3)

	10% PEG 40 μm	10% PEG 80 μm	30% PEG 40 μm	30% PEG 80 μm
Pearson's coeff, R_r	0.83 ± 0.03	0.64 ± 0.12	−0.15 ± 0.20	−0.11 ± 0.16
Manders overlap coeff, R	0.94 ± 0.02	0.83 ± 0.09	0.65 ± 0.03	0.65 ± 0.01
overlap coeff, k_1	0.95 ± 0.11	0.85 ± 0.22	0.67 ± 0.37	0.20 ± 0.12
overlap coeff, k_2	0.93 ± 0.15	0.81 ± 0.10	0.63 ± 0.19	2.10 ± 0.46

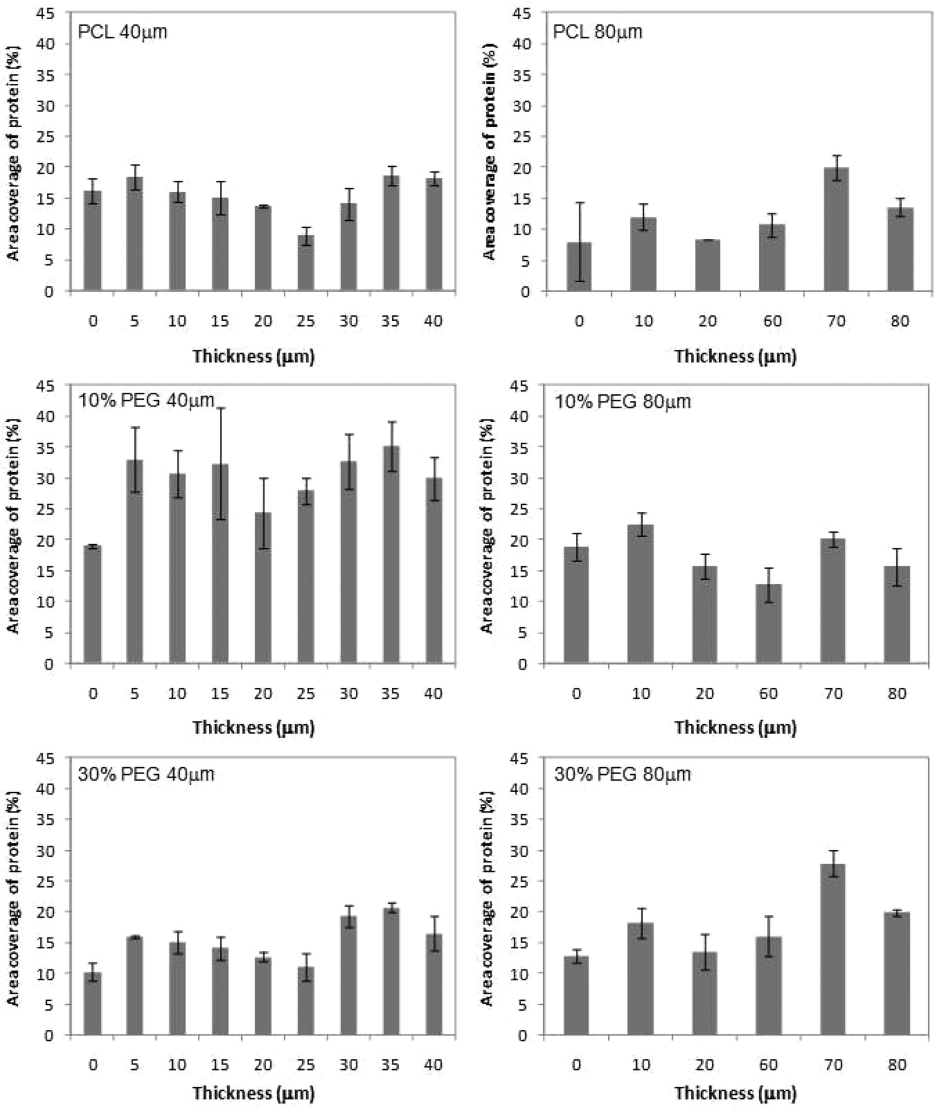

Figure 4. Quantification of protein distribution in terms of the total area coverage of protein-rich domains at specific optical layer. All protein coverage was quantified in triplicate while the data is plotted as mean ± standard deviation of the mean.

leached out from the polymer films, where the amount of PEG leaching increases with the increasing PEG content, and with the decreasing thickness. Within the first 6 h, approximately 45−65% PEG leached out from 30% PEG blends, while only 16−22% of PEG was released from 10% PEG blends. This was followed by a slower, gradual release.

With the above data, it is clear that the addition of PEG increases the protein burst release. In order to estimate the significance of protein-PEG colocalization and contribution of the PEG leaching rate to the observed release profile, each PEG leaching profile was multiplied by its corresponding Manders overlap coefficient (R) (refer to Table 2: this coefficient is the coefficient of choice for reasons to be discussed in the next section). This allows one to estimate the amount of protein release from PCL/PEG blends. These results were compared with the actual protein release data measured in an independent in vitro release experiment using micro-BCA assay (Figure 6). Interestingly, both sets of the protein release profile were in agreement with each other ($R^2 > 0.92$), with only ∼5−12% deviations observed. Nevertheless, statistical analysis of the differences between the actual and estimated protein release showed $p > 0.05$ in all formulations; this was considered to indicate statistical insignificance in the discrepancy, which is confirmed by the overlapping error bars in most of the release time point.

dx.doi.org/10.1021/mp200513b|Mol. Pharmaceutics 2011, 8, 2173−2182

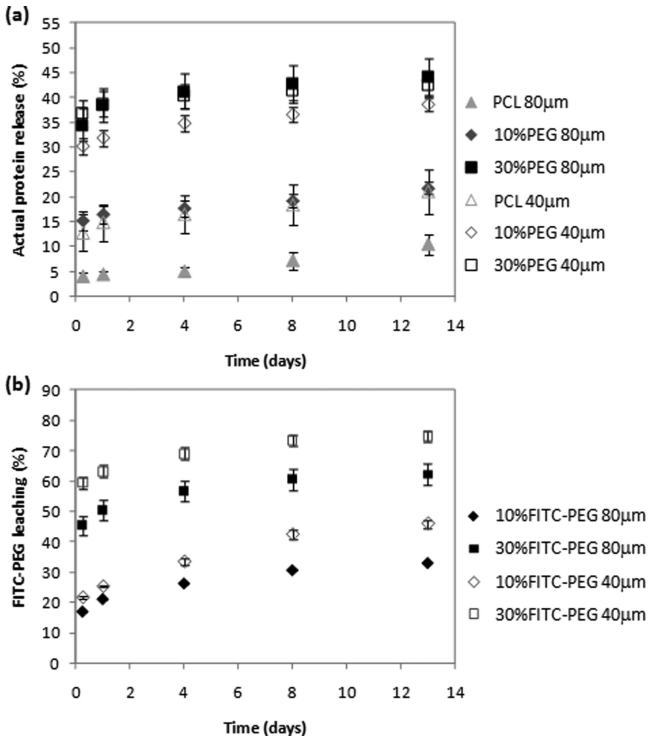

Figure 5. In vitro release studies for actual protein release (a) and PEG leaching (b) in PBS at 37 °C. All formulations were tested in triplicate while the data is presented as mean ± standard deviation of the mean.

DISCUSSION

PCL, a biodegradable polymer, has been extensively studied for its application in protein delivery. Due to its high degree of hydrophobicity and crystallinity, PCL degrades very slowly and results in a slow release rate of slowly diffusing species, such as proteins.[44−46] Several approaches have been used to modify protein release rate. These include blending the hydrophobic matrix with polymers of greater hydrophilicity, such as PEG. For such blends, it has been proposed that the drug/protein release is purely diffusion-controlled, either in a Fickian or a non-Fickian diffusion mode, through pores formed by the leached-out PEG.[4,7,8,10] The PEG aggregates presented on the surfaces were dissolved and leached out from the matrix when contacted with an aqueous medium; pores were consequently formed and filled with water to allow drug/protein release. In this paper, we refer to this release mechanism as a "pore-diffusion model". Despite the extensive studies of PEG blend systems and the development of mathematical models, the release mechanisms remain incompletely understood. Hence, the goal of this study was to explore the underlying protein release mechanisms from the perspective of protein distribution and its partitioning in a phase separated PCL/PEG blend.

Confocal Raman mapping and CLSM imaging were used in conjunction to investigate protein distribution in PCL/PEG blends. Qualitative analysis of Raman mapping showed phase segregation of polymers, where PEG was separated into individual domains from the PCL continuous matrix, forming PEG-rich islands. This is in agreement with the DSC results that indicate the immiscibility between the crystalline phase of PCL and PEG. Interestingly, the mapped image for protein showed a similar phase separated pattern that replicated the

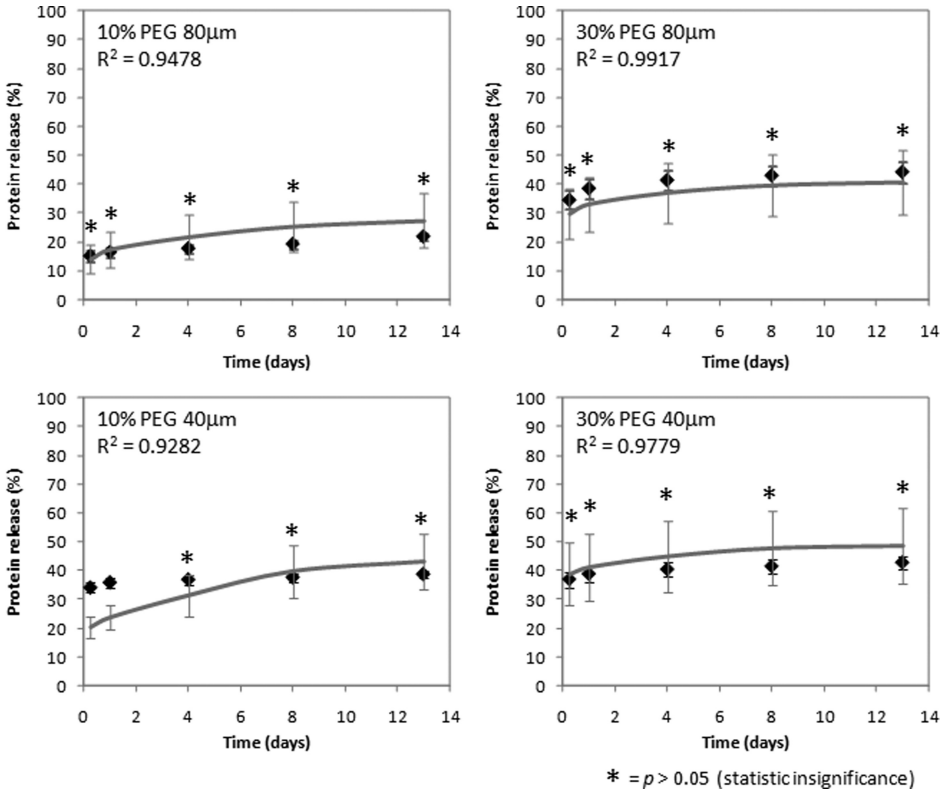

Figure 6. Comparison between actual (black diamonds) and estimated (gray lines) protein release profile. Statistical analysis was performed using *t*-test, and the probability value of $p > 0.05$ was considered to indicate statistical insignificance.

dx.doi.org/10.1021/mp200513b|*Mol. Pharmaceutics* 2011, 8, 2173−2182

mapped image of PEG, indicating colocalization of protein-PEG in the same domain. To date, colocalization of protein and PEG has not been reported qualitatively or quantitatively; hence, in addition to Raman mapping, CLSM imaging was also carried out using fluorescence-tagged PEG and protein, to quantify the colocalization. Both sets of imaging confirmed extensive protein-PEG colocalization.

Image processing of dual channel fluorescence microscopic images further quantifies the amount of colocalized domain, as described by a few coefficients. The resulting Pearson's coefficients for 10% PEG blends indicate a positive correlation between protein-PEG overlapping domain and a high degree of colocalization. However, the negative value of Pearson's coefficients for 30% PEG blends need not imply an inverse correlation. According to a review by Zinchuk et al.,[47] negative values of Pearson's correlation should be interpreted very cautiously. Manders overlap coefficient should be employed if the intensity of one component is stronger than the others, as it allows quantification of colocalization coefficients in such images more reliably. In addition, Bolte et al.[34] assessed the use of Pearson's correlation in four different colocalization situations (complete colocalization, complete colocalization with different intensities, partial colocalization, and exclusion) and concluded that Pearson's correlation coefficient values point to colocalization (value close to 1) when the images of two color channels are completely colocalized; however, this correlation rarely discriminates the differences between partial colocalization and exclusion. The authors state, "Values other than those close to 1 and especially mid-range coefficients (−0.5 to 0.5) do not allow conclusions to be drawn." The evaluation of colocalization using Pearson's correlation may be ambiguous in our case, probably due to the variations in fluorescence intensities, noise, and heterogeneous colocalization relationship between protein and PEG. Hence, only Manders coefficients were used to estimate protein release from PCL/PEG blends in the subsequent analysis.

From Manders coefficients, the degree of protein-PEG colocalization was found to be higher for 10% PEG blends (83%−94%) compared to 30% PEG blend systems (65%). At present, we do not have an explanation for this observation. It may be related to the solubility limit of protein in PEG-containing solutions.[6,8,48,49] Herrmann et al.[6] performed a solubility test of protein (IFN-α) in concentrated aqueous PEG 6000 solutions. In this study, IFN-α spontaneously crystallized in PEG 6000 concentration above 3%, and almost negligible protein solubility at PEG concentration above 10%. A similar phenomenon may account for our observations here with respect to lysozyme solubility in PEG 2000 at 10% PEG in PCL and at 30% PEG in PCL, although the two systems are not strictly comparable.

In order to examine the effect of film thickness on protein release rate, we fabricated protein loaded films of 40 and 80 μm at the same protein loading. As expected, almost all of the 40 μm films exhibited a higher protein release rate, likely due to a faster water penetration rate in a thinner film as compared to the 80 μm formulations. Blends with 30% PEG loading, however, exhibited similar protein release rate for both thicknesses. To explain these observations, protein distribution of all formulations was investigated via our novel image processing method. Quantitative analysis of protein distribution showed homogeneous distribution throughout the entire film, independent of PEG contents. Therefore, the presence of different PEG loading did not substantially alter the distribution of protein within the thickness of the film. However, film thickness was found to have a slight effect on protein distribution whereby the protein coverage for the 40 μm films was slightly higher than the 80 μm formulations for PCL and 10% PEG loading. This could account for the increase in protein release rate, in addition to the higher water penetration rate mentioned earlier. On the other hand, similar protein coverage was observed for 30% PEG loading for both film thicknesses, thus accounting for the lack of dependence of release on thickness in this case.

From the in vitro release studies, the addition of PEG significantly amplified the magnitude of burst effect and total amount of released protein. Similar findings were observed by other research groups.[4,5,7,8,10,14−16] In most cases, the effect of protein burst release was attributed to surface segregation or loosely bound protein at the surface layer. However, in our system, we have shown that the proteins do not accumulate on the surface; thus another cause must be sought for the increased burst and subsequent release of protein. To answer this question, PEG leaching was also quantified as a function of time. Combining the overlapping coefficient according to Manders together with the PEG leaching data, a comparison was made between the estimated protein release, to the actual protein release profile measured by BCA analysis. Clearly, good agreement was obtained between calculated and experimental release. What this implies is that the release of protein is dominated by the release of PEG with associated protein. The other contributions to the burst and subsequent release, such as surface segregation, or diffusion through the PCL matrix, are not significant in this system. Thus, the picture that emerges is shown in Figure 7: when PCL/PEG films are exposed to aqueous media, there is an initial burst release of PEG together with the colocalized proteins. Voids, which were formed by the leaching of PEG, later facilitated the diffusion of PEG entrapped deeper in the film matrix (but also associated with protein) and hence increased the overall rate and amount of protein released. Non-colocalized protein, on the other hand, permeated much more slowly through the highly crystalline matrix. Incomplete protein release in all formulations is understandable as the PEG/proteins embedded deeper within the bulk were not expected to be released until complete biodegradation of PCL occurs or until all pores became interconnected.

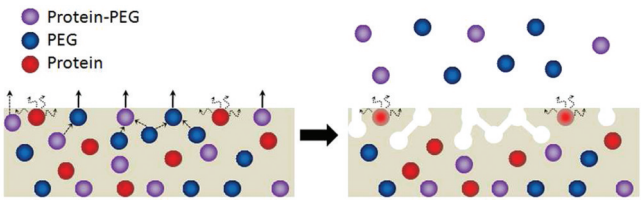

Figure 7. Cartoon of protein release mechanism in PCL/PEG blend films.

So does this proposed mechanism vary appreciably from the "pore-diffusion model"? Does our colocalization data distinguish sufficiently between the two? In the "pore-diffusion model", PEG leaches out first, creating water-filled pores which then allow easier diffusion of protein. In this model, the initial burst is due mostly to undissolved protein at the surface. In comparison in our colocalization model, the initial burst is due to a burst of PEG release, which carries with its associated

protein. This is responsible not only for the initial burst but also for subsequent release. Our CLSM data clearly shows that there is no surface segregation, hence ruling out this as a cause of the burst. Following burst, the PEG release rate is similar regardless of PEG content or film thickness. This similarity is also reflected in the protein release rates, which affirms that the entire release profile reflects the release of PEG from the film, carrying with it the colocalized protein. The rather close fitting of the experimental release curves using the Manders coefficients (R) clearly supports our model for both phases of release, but cannot rule out the possibility of diffusion through aqueous pore channels. To distinguish between the two possibilities, it is necessary to study a leachant which associates less with the protein. This study is being planned.

On a practical level, the ability to visualize and quantify protein-PEG colocalization via our novel image processing technique has provided a new platform for understanding the release mechanism from the aspect of protein partitioning. It should be noted that the protein-PEG colocalization coefficients calculated from this work may not be generalized to all protein loaded PEG-based blends delivery systems, i.e. for a different protein or a different PEG in a PCL/PEG blend system. However, we maintain that colocalization of protein into the PEG in a phase separated PEG blend is the driving factor in protein release. As such the concept should be applicable to different geometries, such as fibers or microspheres, provided the PEG is phase separated, and has a higher solubility for protein than the dispersing phase. If it is possible to quantify the extent of colocalization by a suitable technique, and if the PEG leaching can be measured or predicted, then the protein release mechanism can be predicted. It is hoped that this predictive capability allows for manipulation of formulations to attain a desired protein release profile. In the past, it has been almost impossible to quantify protein/drug partitioning into each phase of a blended system, without destroying the samples. Using our approach, the distribution of protein throughout a given sample can be quantified, although this method does not yield quantitative compositional data (as given by ESCA and XPS) for the mass of protein distributed as a function of depth. The sample depth over which our method works depends on the materials used; in this work, protein distribution up to a depth of ~25 μm can be analyzed. As compared with the currently available quantification instruments that are limited to <100 nm,[17,18] this larger analysis volume resulted in higher accuracy and may lead to wider applications in drug/protein delivery systems.

CONCLUSIONS

The distribution of PEG and protein in PCL/PEG blends was visualized by confocal Raman and CLSM. From both imaging methods, PEG segregation was observed in all of the PCL/PEG blends, and more importantly, protein was found to partition preferentially into the hydrophilic PEG domains. Quantification of protein-PEG colocalization by image processing enabled the prediction of protein release when coupled with PEG leaching. This novel approach was found to be in good agreement with the experimental data, highlighting the role of protein-PEG colocalization in protein transport mechanisms.

ASSOCIATED CONTENT

Supporting Information

FITC-PEG calibration curve. This material is available free of charge via the Internet at http://pubs.acs.org.

AUTHOR INFORMATION

Corresponding Author

*Phone: +65 6790 4259. Fax: +65 6790 9081. E-mail: assubbu@ntu.edu.sg. School of Materials Science and Engineering, Nanyang Technological University, Block N4.1-02-06, Nanyang Avenue, Singapore 639798.

ACKNOWLEDGMENTS

This work was supported by a grant from National Research Foundation (NRF)—Competitive Research Programme (CRP). Authors thank Dr. Ma Lwin Lwin and Ms. Xia Yun for their knowledge in image processing and Dr. Terry W. J. Steele for fruitful discussions.

REFERENCES

(1) Bei, J.; Wang, W.; Wang, Z.; Wang, S. Surface properties and drug release behaviour of polycaprolactone polyether blend and copolymer. *Polym. Adv. Technol.* **1996**, *7*, 104−107.

(2) Jiang, W. L.; Schwendeman, S. P. Stabilization and controlled release of bovine serum albumin encapsulated in poly(D, L-lactide) and poly(ethylene glycol) microsphere blends. *Pharm. Res.* **2001**, *18*, 878−885.

(3) Cleek, R. L.; Ting, K. C.; G. Eskin, S.; Mikos, A. G. Microparticles of poly(dl-lactic-co-glycolic acid)/poly(ethylene glycol) blends for controlled drug delivery. *J. Controlled Release* **1997**, *48*, 259−268.

(4) Lin, W.-J.; Lee, H.-G. Design of a microporous controlled delivery system for theophylline tablets. *J. Controlled Release* **2003**, *89*, 179−187.

(5) Zhang, Y. Z.; Wang, X.; Feng, Y.; Li, J.; Lim, C. T.; Ramakrishna, S. Coaxial electrospinning of (fluorescein isothiocyanate-conjugated bovine serum albumin)-encapsulated poly(ε-caprolactone) nanofibers for sustained release. *Biomacromolecules* **2006**, *7*, 1049−1057.

(6) Herrmann, S.; Mohl, S.; Siepmann, F.; Siepmann, J.; Winter, G. New insight into the role of polyethylene glycol acting as protein release modifier in lipidic implants. *Pharm. Res.* **2007**, *24*, 1527−1537.

(7) Herrmann, S.; Winter, G.; Mohl, S.; Siepmann, F.; Siepmann, J. Mechanisms controlling protein release from lipidic implants: Effects of PEG addition. *J. Controlled Release* **2007**, *118*, 161−168.

(8) Siepmann, F.; Herrmann, S.; Winter, G.; Siepmann, J. A novel mathematical model quantifying drug release from lipid implants. *J. Controlled Release* **2008**, *128*, 233−240.

(9) Koennings, S.; Tessmar, J.; Blunk, T.; Gopferich, A. Confocal microscopy for the elucidation of mass transport mechanisms involved in protein release from lipid-based matrices. *Pharm. Res.* **2007**, *24*, 1325−1335.

(10) Verhoeven, E.; Siepmann, F.; De Beer, T. R. M.; Van Loo, D.; Van den Mooter, G.; Remon, J. P.; Siepmann, J.; Vervaet, C. Modeling drug release from hot-melt extruded mini-matrices with constant and non-constant diffusivities. *Eur. J. Pharm. Biopharm.* **2009**, *73*, 292−301.

(11) Kim, J. K.; Taki, K.; Nagamine, S.; Ohshima, M. Periodic porous stripe patterning in a polymer blend film induced by phase separation during spin-casting. *Langmuir* **2008**, *24*, 8898−8903.

(12) Kim, J.-K.; Taki, K.; Ohshima, M. Preparation of a unique microporous structure via two step phase separation in the course of drying a ternary polymer solution. *Langmuir* **2007**, *23*, 12397−12405.

(13) Chuang, W.-T.; Shih, K.-S.; Hong, P.-D. Kinetics of phase separation in poly(ε-caprolactone)/poly(ethylene glycol) blends. *J. Polym. Res.* **2005**, *12*, 197−204.

(14) Cheng, L.; Lei, L.; Guo, S. In vitro and in vivo evaluation of praziquantel loaded implants based on PEG/PCL blends. *Int. J. Pharm.* **2010**, *387*, 129−138.

(15) Kim, T. G.; Lee, D. S.; Park, T. G. Controlled protein release from electrospun biodegradable fiber mesh composed of poly(ε-caprolactone) and poly(ethylene oxide). *Int. J. Pharm.* **2007**, *338*, 276−283.

(16) Windbergs, M.; Strachan, C. J.; Kleinebudde, P. Tailor-made dissolution profiles by extruded matrices based on lipid polyethylene glycol mixtures. *J. Controlled Release* **2009**, *137*, 211−216.
(17) Belu, A.; Mahoney, C.; Wormuth, K. Chemical imaging of drug eluting coatings: Combining surface analysis and confocal Raman microscopy. *J. Controlled Release* **2008**, *126*, 111−121.
(18) Rafati, A.; Davies, M. C.; Shard, A. G.; Hutton, S.; Mishra, G.; Alexander, M. R. Quantitative XPS depth profiling of codeine loaded poly(l-lactic acid) films using a coronene ion sputter source. *J. Controlled Release* **2009**, *138*, 40−44.
(19) Lao, L. L.; Venkatraman, S. S. Adjustable paclitaxel release kinetics and its efficacy to inhibit smooth muscle cells proliferation. *J. Controlled Release* **2008**, *130*, 9−14.
(20) Wang, X. T.; Venkatraman, S.; Boey, F.; Loo, S. C.; Tan, L. P. Effects of controlled-released sirolimus from polymer matrices on human coronary artery smooth muscle cells. *J. Biomater. Sci., Polym. Ed.* **2007**, *18*, 1401−1414.
(21) Huang, Y.; Venkatraman, S. S.; Boey, F. Y. C.; Lahti, E. M.; Umashankar, P. R.; Mohanty, M.; Arumugam, S.; Khanolkar, L.; Vaishnav, S. In vitro and in vivo performance of a dual drug-eluting stent (DDES). *Biomaterials* **2010**, *31*, 4382−4391.
(22) Kang, E.; Robinson, J.; Park, K.; Cheng, J.-X. Paclitaxel distribution in poly(ethylene glycol)/poly(lactide-co-glycolic acid) blends and its release visualized by coherent anti-Stokes Raman scattering microscopy. *J. Controlled Release* **2007**, *122*, 261−268.
(23) Kang, E. N.; Wang, H. F.; Kwon, I. K.; Robinson, J.; Park, K.; Cheng, J. X. In situ visualization of paclitaxel distribution and release by coherent anti-stokes Raman scattering microscopy. *Anal. Chem.* **2006**, *78*, 8036−8043.
(24) Windbergs, M.; Jurna, M.; Offerhaus, H. L.; Herek, J. L.; Kleinebudde, P.; Strachan, C. J. Chemical imaging of oral solid dosage forms and changes upon dissolution using coherent anti-Stokes Raman scattering microscopy. *Anal. Chem.* **2009**, *81*, 2085−2091.
(25) White, N. S.; Errington, R. J. Fluorescence techniques for drug delivery research: theory and practice. *Adv. Drug Delivery Rev.* **2005**, *57*, 17−42.
(26) Pygall, S. R.; Whetstone, J.; Timmins, P.; Melia, C. D. Pharmaceutical applications of confocal laser scanning microscopy: The physical characterisation of pharmaceutical systems. *Adv. Drug Delivery Rev.* **2007**, *59*, 1434−1452.
(27) Verhoogt, H.; van Dam, J.; de Boer, A. P.; Draaijer, A.; Houpt, P. M. Confocal laser scanning microscopy: A new method for determination of the morphology of polymer blends. *Polymer* **1993**, *34*, 1325−1329.
(28) Determan, A. S.; Trewyn, B. G.; Lin, V. S. Y.; Nilsen-Hamilton, M.; Narasimhan, B. Encapsulation, stabilization, and release of BSA-FITC from polyanhydride microspheres. *J. Controlled Release* **2004**, *100*, 97−109.
(29) Rafati, H.; Coombes, A. G. A.; Adler, J.; Holland, J.; Davis, S. S. Protein-loaded poly(-lactide-co-glycolide) microparticles for oral administration: formulation, structural and release characteristics. *J. Controlled Release* **1997**, *43*, 89−102.
(30) Widjaja, E.; Li, C.; Chew, W.; Garland, M. Band-target entropy minimization. A robust algorithm for pure component spectral recovery. Application to complex randomized mixtures of six components. *Anal. Chem.* **2003**, *75*, 4499−4507.
(31) Li, C.; Widjaja, E.; Chew, W.; Garland, M. Rhodium tetracarbonyl hydride: The elusive metal carbonyl hydride13. *Angew. Chem., Int. Edit.* **2002**, *41*, 3785−3789.
(32) Seah, R. K. H.; Garland, M.; Loo, J. S. C.; Widjaja, E. Use of Raman microscopy and multivariate data analysis to observe the biomimetic growth of carbonated hydroxyapatite on bioactive glass. *Anal. Chem.* **2009**, *81*, 1442−1449.
(33) Widjaja, E.; Seah, R. K. H. Application of Raman microscopy and band-target entropy minimization to identify minor components in model pharmaceutical tablets. *J. Pharm. Biomed. Anal* **2008**, *46*, 274−281.
(34) Bolte, S.; Cordelières, F. P. A guided tour into subcellular colocalization analysis in light microscopy. *J. Microsc.* **2006**, *224*, 213−232.
(35) Manders, E. M. M.; Stap, J.; Brakenhoff, G. J.; Van Driel, R.; Aten, J. A. Dynamics of three-dimensional replication patterns during the S-phase, analysed by double labelling of DNA and confocal microscopy. *J. Cell Sci.* **1992**, *103*, 857−862.
(36) Manders, E. M. M.; Verbeek, F. J.; Aten, J. A. Measurement of co-localization of objects in dual-colour confocal images. *J. Microsc.* **1993**, *169*, 375−382.
(37) Coleman, M. M.; Zarian, J. Fourier-transform infrared studies of polymer blends. II. Poly(ε-caprolactone)-poly(vinyl chloride) system. *J. Polym. Sci., Part B: Polym. Phys.* **1979**, *17*, 837−850.
(38) Widjaja, E.; Lee, W. L.; Loo, S. C. J. Application of Raman Microscopy to Biodegradable Double-Walled Microspheres. *Anal. Chem.* **2010**, *82*, 1277−1282.
(39) Mohan Misra, R.; Agarwal, R.; Tandon, P.; Dayal Gupta, V. Phonon dispersion and heat capacity in poly(ε-caprolactone). *Eur. Polym. J.* **2004**, *40*, 1787−1798.
(40) Kister, G.; Cassanas, G.; Bergounhon, M.; Hoarau, D.; Vert, M. Structural characterization and hydrolytic degradation of solid copolymers of d,l-lactide-co-ε-caprolactone by Raman spectroscopy. *Polymer* **2000**, *41*, 925−932.
(41) Yoshihara, T.; Tadokoro, H.; Murahashi, S. Normal vibrations of the polymer molecules of helical conformation. IV. polyethylene oxide and polyethylene-d_4 oxide. *J. Chem. Phys.* **1964**, *41*, 2902.
(42) Maxfield, J.; Shepherd, I. W. Conformation of poly(ethylene oxide) in the solid state, melt and solution measured by Raman scattering. *Polymer* **1975**, *16*, 505−509.
(43) Krimm, S.; Bandekar, J.; C.B. Anfinsen, J. T. E.; Frederic, M. R., Vibrational spectroscopy and conformation of peptides, polypeptides, and proteins. In *Advances in protein chemistry*; Academic Press: 1986; Vol. Vol. *38*, pp 181−364.
(44) Chandra, R.; Rustgi, R. Biodegradable polymers. *Prog. Polym. Sci.* **1998**, *23*, 1273−1335.
(45) Nair, L. S.; Laurencin, C. T. Biodegradable polymers as biomaterials. *Prog. Polym. Sci.* **2007**, *32*, 762−798.
(46) Woodruff, M. A.; Hutmacher, D. W. The return of a forgotten polymer--Polycaprolactone in the 21st century. *Prog. Polym. Sci.* **2010**, *35*, 1217−1256.
(47) Zinchuk, V.; Zinchuk, O.; Okada, T. Quantitative colocalization analysis of multicolor confocal immunofluorescence microscopy images: Pushing pixels to explore biologocal phenomena. *J. Histochem. Cytochem.* **2007**, *40*, 101−111.
(48) Atha, D. H.; Ingham, K. C. Mechanism of precipitation of proteins by polyethylene glycols - analysis in terms of excluded volume. *J. Biol. Chem.* **1981**, *256*, 2108−2117.
(49) Shulgin, I. L.; Ruckenstein, E. Preferential hydration and solubility of proteins in aqueous solutions of polyethylene glycol. *Biophys. Chem.* **2006**, *120*, 188−198.